



## ISTITUTO NAZIONALE DI RICERCA METROLOGICA Repository Istituzionale

Simple-design ultra-low phase noise microwave frequency synthesizers for high-performing Cs and Rb vapor-cell atomic clocks

*Original*

Simple-design ultra-low phase noise microwave frequency synthesizers for high-performing Cs and Rb vapor-cell atomic clocks / Francois, B; Calosso, Ce; Hafiz, Ma; Micalizio, Salvatore; Boudot, R.. - In: REVIEW OF SCIENTIFIC INSTRUMENTS. - ISSN 0034-6748. - 86:094707(2015).

*Availability:*

This version is available at: 11696/30128 since: 2021-01-29T16:28:46Z

*Publisher:*

AIP

*Published*

DOI:

*Terms of use:*

This article is made available under terms and conditions as specified in the corresponding bibliographic description in the repository

*Publisher copyright*

(Article begins on next page)

# Simple-design ultra-low phase noise microwave frequency synthesizers for high-performing Cs and Rb vapor-cell atomic clocks

Cite as: Rev. Sci. Instrum. **86**, 094707 (2015); <https://doi.org/10.1063/1.4929384>

Submitted: 16 June 2015 . Accepted: 11 August 2015 . Published Online: 24 September 2015

B. François, C. E. Calosso, M. Abdel Hafiz, S. Micalizio, and R. Boudot



View Online



Export Citation



CrossMark

## ARTICLES YOU MAY BE INTERESTED IN

[A low phase noise microwave frequency synthesis for a high-performance cesium vapor cell atomic clock](#)

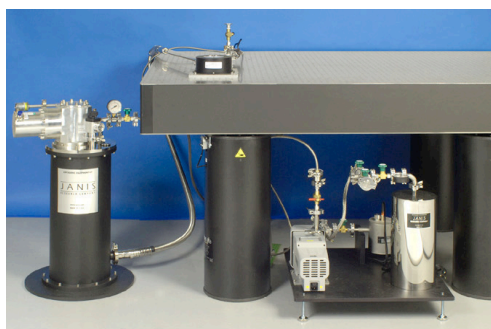
Review of Scientific Instruments **85**, 094709 (2014); <https://doi.org/10.1063/1.4896043>

[A high-performance Raman-Ramsey Cs vapor cell atomic clock](#)

Journal of Applied Physics **121**, 104903 (2017); <https://doi.org/10.1063/1.4977955>

[Development of low phase noise microwave frequency synthesizers for reducing Dick effect of Cs fountain clocks](#)

AIP Advances **8**, 095311 (2018); <https://doi.org/10.1063/1.5042492>



**JANIS**  
A LAKE SHORE COMPANY

**Rising LHe costs? Janis has a solution.**  
Janis' Recirculating Cryocooler eliminates the use of Liquid Helium for "wet" cryogenic systems.

[sales@lakeshore.com](mailto:sales@lakeshore.com) [www.lakeshore.com/rgc](http://www.lakeshore.com/rgc) Click for more information.

# Simple-design ultra-low phase noise microwave frequency synthesizers for high-performing Cs and Rb vapor-cell atomic clocks

B. François,<sup>1,2</sup> C. E. Calosso,<sup>2</sup> M. Abdel Hafiz,<sup>1</sup> S. Micalizio,<sup>2</sup> and R. Boudot<sup>1</sup>

<sup>1</sup>FEMTO-ST, CNRS, Université de Franche-Comté, 26 chemin de l'Épithaphe, 25030 Besançon, France

<sup>2</sup>INRIM, Strada delle Cacce 91, 10135 Torino, Italy

(Received 16 June 2015; accepted 11 August 2015; published online 24 September 2015)

We report on the development and characterization of novel 4.596 GHz and 6.834 GHz microwave frequency synthesizers devoted to be used as local oscillators in high-performance Cs and Rb vapor-cell atomic clocks. The key element of the synthesizers is a custom module that integrates a high spectral purity 100 MHz oven controlled quartz crystal oscillator frequency-multiplied to 1.6 GHz with minor excess noise. Frequency multiplication, division, and mixing stages are then implemented to generate the exact output atomic resonance frequencies. Absolute phase noise performances of the output 4.596 GHz signal are measured to be  $-109$  and  $-141$  dB rad<sup>2</sup>/Hz at 100 Hz and 10 kHz Fourier frequencies, respectively. The phase noise of the 6.834 GHz signal is  $-105$  and  $-138$  dB rad<sup>2</sup>/Hz at 100 Hz and 10 kHz offset frequencies, respectively. The performances of the synthesis chains contribute to the atomic clock short term fractional frequency stability at a level of  $3.1 \times 10^{-14}$  for the Cs cell clock and  $2 \times 10^{-14}$  for the Rb clock at 1 s averaging time. This value is comparable with the clock shot noise limit. We describe the residual phase noise measurements of key components and stages to identify the main limitations of the synthesis chains. The residual frequency stability of synthesis chains is measured to be at the  $10^{-15}$  level for 1 s integration time. Relevant advantages of the synthesis design, using only commercially available components, are to combine excellent phase noise performances, simple-architecture, low-cost, and to be easily customized for signal output generation at 4.596 GHz or 6.834 GHz for applications to Cs or Rb vapor-cell frequency standards. © 2015 AIP Publishing LLC. [<http://dx.doi.org/10.1063/1.4929384>]

## I. INTRODUCTION

Atomic frequency standards provide the ultimate source of accuracy and stability for all modern communication, navigation, and timekeeping systems, and nowadays commercially available devices are deployed in many strategic industrial fields. In this domain, microwave vapor-cell atomic clocks, mainly commercially available Rb clocks,<sup>1,2</sup> are known to be valuable candidates because they combine compactness, reliability, low power consumption, and excellent fractional frequency stability at the level of  $10^{-11} \tau^{-1/2}$  for integration times  $\tau$  up to 10 000 s. Nevertheless, more stable clocks are required in order to match modern industrial demands and technical applications such as next-generation satellite-based navigation systems. Recently, due to better performing laser sources and to innovative techniques to prepare and detect the atoms, several cell-based atomic clock prototypes exhibiting unprecedented frequency stability have been developed. Université de Neuchâtel (UNINE) has developed a compact high-performance continuous-regime double-resonance rubidium standard with a short term fractional frequency stability of  $1.4 \times 10^{-13} \tau^{-1/2}$  up to averaging time  $\tau = 100$  s.<sup>3</sup> More recently, they demonstrated a pulsed optically pumped (POP) Rb clock based on a compact magnetron-type microwave cavity with a frequency stability at the level of  $2.1 \times 10^{-13} \tau^{-1/2}$  up to  $\tau = 30$  s.<sup>4</sup> At the Italian metrological institute (INRIM), they proposed and demonstrated a POP Rb frequency standard with optical detection with a fractional frequency stability of  $1.7 \times 10^{-13} \tau^{-1/2}$  up to 10 000 s integration time.<sup>5</sup> At LNE-SYRTE

(Observatoire de Paris), they developed a Raman-Ramsey Cs vapor-cell atomic clock based on coherent population trapping (CPT)<sup>6</sup> that achieves a short-term frequency stability at the level of  $3.2 \times 10^{-13} \tau^{-1/2}$  up to 1000 s averaging time.<sup>7</sup> At FEMTO-ST, using the push pull optical pumping (PPOP) technique,<sup>8–10</sup> they reported a Cs CPT clock with a short-term fractional frequency stability of  $3 \times 10^{-13} \tau^{-1/2}$  up to 100 s averaging time.<sup>11</sup> These impressive performances, about two orders of magnitude better than standard commercial Rb clocks, clearly make this technology competitive with best compact cold-atom clocks<sup>12,13</sup> or even with passive hydrogen masers<sup>14</sup> up to 10 000 s integration time for greatly reduced volume and power consumption.

In passive atomic frequency standards, the atoms are interrogated periodically and the control signal of the slaved local oscillator (LO) is updated at equally spaced time intervals. It has been shown that the lack of information on the frequency of the LO caused by the sampling process can lead to a limitation of the short-term frequency stability of the atomic standard. This effect, known as intermodulation effect,<sup>15</sup> originates from the down-conversion of the LO intrinsic frequency noise at Fourier frequencies higher than the interrogation frequency in the resonator bandwidth. Later, it was shown that the main contribution was related to the noise associated at the second harmonic of the modulation frequency.<sup>16</sup> The intermodulation effect is known as Dick effect for clocks working in pulsed operation.<sup>17,18</sup> More recently, a detailed and interesting analysis of the Dick effect in pulsed CPT-based vapor-cell clocks was reported in Ref. 7, revealing, compared to traditional





FIG. 2. Photograph of a 100 MHz-1.6 GHz XM16 Pascall frequency-multiplication module.

driver and key element of the synthesis chain is a custom-designed XM16 Pascall module,<sup>22</sup> shown on Fig. 2. It integrates an ultra-low phase noise 100 MHz OCXO (Pascall OCXOF-E-100) and a frequency multiplication stage to produce a low noise 1.6 GHz output signal with a power of 13 dBm. Figure 3 reports a simplified schematic of the XM16 module. This module uses a low noise 100 MHz OCXO whose maintaining circuit is designed such that the close-in phase noise of the oscillator is determined by the quartz crystal resonator.<sup>23</sup> The latter, a 5th-overtone stress-compensated (SC, Ref. 24)-cut crystal with a 4-point mount package for low vibration sensitivity, has been selected in order to meet our specifications. For this purpose, the crystal is initially measured in a test-oscillator and graded according to phase noise results. The tuning range of the OCXO is higher than 6 ppm at 100 MHz for a 0-10 V input range. The OCXO exhibits a typical long-term frequency aging of  $10^{-7}$ /yr, with 10 yr of operation expected. Multiplication to 1.6 GHz is performed thanks to three multiplication stages, with bandpass filtering and amplification at each step to maintain low noise floor and to keep a low level of spurious 100 MHz harmonics. Heterojunction bipolar transistors (HBTs)-based amplifiers are used to minimize excess flicker noise. Multipliers are

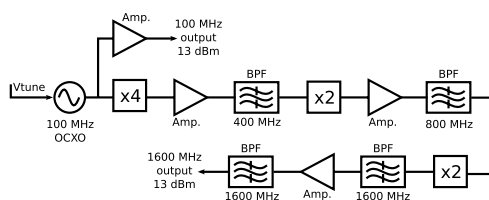


FIG. 3. Simplified schematic of the Pascall XM16 module. The 100 MHz signal is frequency-multiplied to 1.6 GHz using three multiplication modules based on Schottky diode doublers. Before each stage, the signal is band-pass filtered and amplified in order to drive multiplication modules with the appropriate level.

based on passive doublers using Schottky diodes in order to minimize conversion losses and to maximize the power into the following amplifier. This allows to reduce the noise figure of each new amplifier stage. The module is designed in order to minimize leakages between sections and to achieve extremely low sub-harmonics spurious level. Each stage uses its local voltage regulation, with particular attention paid to minimize low-frequency noise on the oscillator supply.

Three XM16 modules, named XM16-264, XM16-265, and XM16-266, expected to be identical, were bought, tested, and compared. As reported later, we observed that the XM16-265 module exhibits significantly better performances, mainly in the 500 Hz-30 kHz range.

The output 1.6 GHz signal is bandpass-filtered with a 50 MHz-bandwidth bandpass filter and power-split into different arms. In the first arm, the 1.6 GHz signal is frequency multiplied to a frequency of 4.8 GHz with a low noise passive frequency multiplier (Minicircuits ZX90-3-452-S+). The output signal is amplified with a 13 dB-gain microwave amplifier (Hittite HMC606), bandpass-filtered, and isolated with a microwave isolator to prevent feedback. In a second arm, the 1.6 GHz signal is frequency-divided by 9 with a low noise programmable frequency divider (Hittite HMC705) to produce a 177.8 MHz signal that is later bandpass-filtered.

In the third arm, the 1.6 GHz signal is frequency-divided by 2 (Hittite HMC361) to an output frequency of 800 MHz. The 800 MHz signal is used to drive a DDS (AD9910) that generates an output frequency of 25.9 MHz. As explained in Section IV, the choice of the DDS is critical in order to ensure the performances of the synthesis chain. This signal is mixed with the 177.8 MHz output signal in a double balanced mixer (Minicircuits ZFM-2-S+) in order to generate a 203.7 MHz signal, again filtered. The latter is sent into the intermediate frequency (IF) port of a microwave double-balanced mixer (Minicircuits ZX05-14LH-S+) to be mixed with the 4.8 GHz signal and to ensure the generation of the final 4.596 GHz signal. The 203.7 MHz signal is kept below 0 dBm in order to use the microwave mixer in linearity. The purpose is then to control the output power of the synthesis chain by tuning the DDS amplitude. The 4.596 GHz signal is bandpass filtered, isolated, and amplified with a microwave amplifier (Nextec NBL-00426). This signal is later used to drive a pigtailed intensity Mach-Zehnder electro-optic modulator devoted to generate two optical sidebands frequency-separated by 9.192 GHz in CPT-based clock setups.<sup>9-11,25</sup>

## B. Phase noise performances

Most of absolute phase noise measurements reported in this article were performed with the same signal source analyzer (Agilent, now Keysight E5052B) than the one used in Ref. 20. For frequencies higher than 2.5 GHz, the down-converter (E5053B) is used. This device has internal references and uses cross correlation techniques to enhance its sensitivity.<sup>26-28</sup>

Nevertheless, it was demonstrated in Ref. 28 that it exists a set of phase and amplitude conditions where the detection of a measured signal in cross-spectral analysis fails partially or entirely. This phenomenon is mainly induced by the amplitude

noise (AM) to phase noise (PM) conversion of the mixer that leads to a combination of PM and AM noise in the measurement. Depending on the sign of the conversion coefficients, both AM and PM spectra add or subtract each other leading to an over-estimation or under-estimation of the phase noise. This phenomenon can induce bumps and notches on the phase noise spectrum of the device under test. Their level depends on the reference oscillator used in the measurement setup. The lower is the difference between the latter and the device under test, the lower is the contribution of this collapse. In such commercial devices, this phenomenon can explain sometimes the high number of bumps and roll-offs in the 100 Hz–100 kHz frequency range. Indeed, in order to provide a reference oscillator with a wide-band sensitivity, the latter is in general composed of two oscillators (a low frequency oscillator with a low level flicker contribution and an oscillator of higher frequency to ensure a low white phase noise floor) with a servo bandwidth in the concerned frequency range (about a few kHz).

In this study, using the E5052B measurement bench, the signature of the amplitude noise to phase noise conversion (AM-PM) collapse has been observed on each measurement performed with the cross correlation function. For the 100 MHz and the 1.6 GHz signals, the signature is observed by the presence of bumps between 1 kHz and 300 kHz. For frequencies higher than 2.5 GHz (4.596 or 6.834 GHz for example), due to the use of the downconverter, the signature of the collapse has not been observed.

Figure 4 shows the two experimental setups we implemented for the phase noise characterization of the XM16 modules. In the first case (Fig. 4(a)), output signals at 100 MHz or 1.6 GHz are directly sent into the commercial E5052B signal source analyzer for measurement. In the other case (Fig. 4(b)), as demonstrated in Ref. 29), a custom-made cross correlation phase noise measurement system is used. In this setup, the module under test is split into two arms and is phase compared in each arm using a saturated double-balanced mixer to the signal of another XM16 module. Phase lock servo loops with a bandwidth of about 40 Hz are adjusted. Error signals are amplified and analyzed using a cross-spectrum fast Fourier transform (FFT) analyzer in order to extract the absolute phase noise performance of the device under test.

Figure 5 reports the absolute phase noise performances of 100 MHz and 1.6 GHz signals of each XM16 module measured using the setup described in Fig. 4(b). Both XM16-264 and XM16-266 modules exhibit similar phase noise performances at 100 MHz and 1.6 GHz. The XM16-265 module presents better phase noise performances of 2–4 dB, mainly in the 600 Hz–20 kHz offset frequency range, that is a region of great importance for vapor-cell atomic clocks. The best module presents phase noise performances at 100 MHz of  $-143$  and  $-174$  dB rad<sup>2</sup>/Hz at 100 Hz and 10 kHz Fourier frequencies, respectively. Frequency multiplication from 100 MHz to 1.6 GHz induces an expected phase noise increase of about 24 dB, showing that the frequency multiplication process is free from excess of noise. To highlight the collapse signature of the cross-spectral function in the E5052B device, we compare in Fig. 6 the absolute phase noise of the 1.6 GHz signal at the output of the XM16-265 module using both setups of Fig. 4.

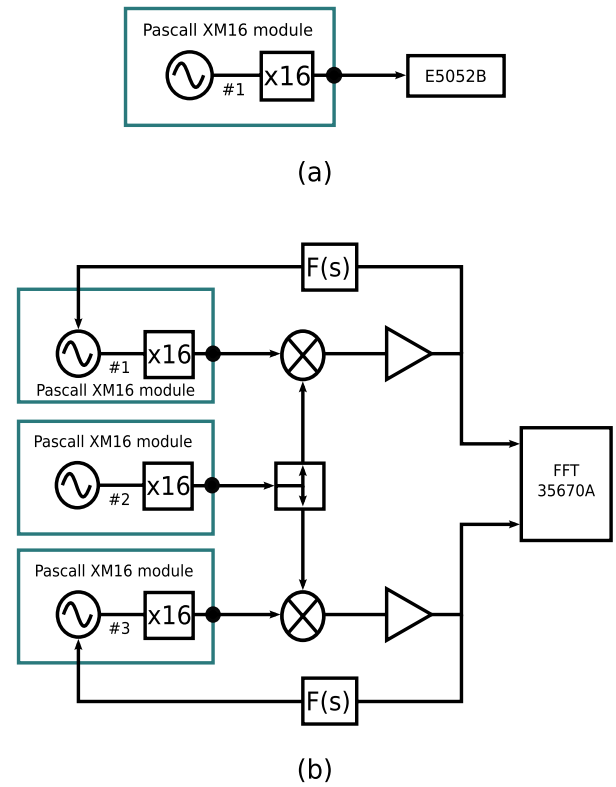


FIG. 4. Experimental setups used for absolute phase noise measurement at 100 MHz and 1.6 GHz. (a) The signal to be measured is directly sent into an Agilent E5052B signal source analyzer using cross correlation techniques. (b) Home-made phase noise measurement setup using a triangulation of high-performance XM16 modules. A FFT-based spectrum analyzer 35670A is used to calculate the phase noise cross-spectrum.

With respect to Fig. 6, the dual channel phase noise measurement is closer to the expected shape of such OCXO. In addition, this measurement is in good agreement with the 4.8 GHz signal phase noise (the cross-spectrum collapse signature has not been observed with the E5053B down-converter). This confirms that the measurement achieved by this setup

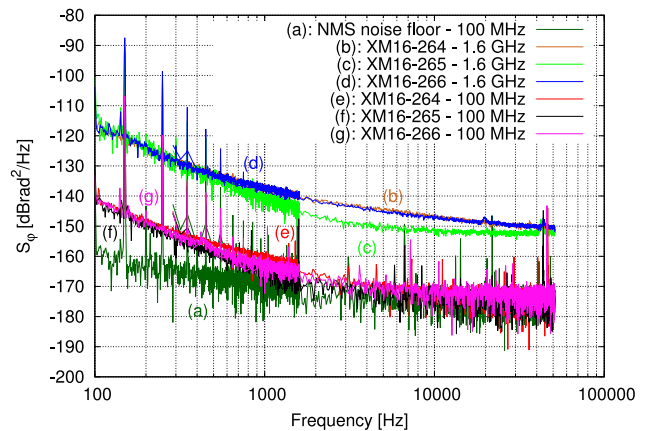


FIG. 5. Absolute phase noise performances at 100 MHz and 1.6 GHz of three XM16 modules. At 1.6 GHz, we report (b) XM16-264, (c) XM16-265, (d) XM16-266. At 100 MHz, we report (e) XM16-264, (f) XM16-265, (g) XM16-266. The Noise Measurement System (NMS) floor has been reported as (a). The XM16-265 module is found to exhibit better performances than the two other units. The setup described in Fig. 4(b) is used.

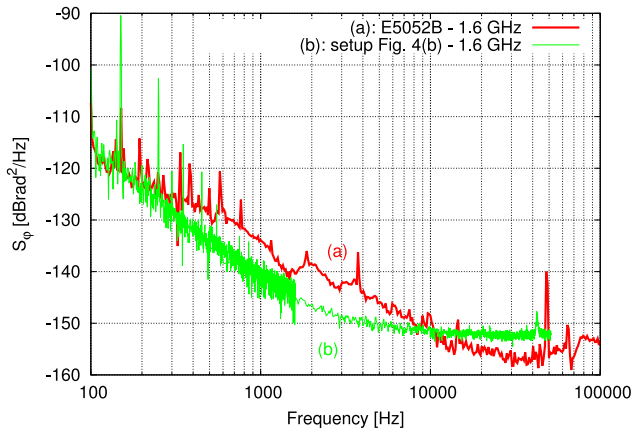


FIG. 6. Absolute phase noise of the 1.6 GHz signal at the output of XM16-265 module. Comparison of the spectrum obtained with setups described in Figure 4. (a) Agilent E5052B, (b) home-made system. For (a), the number of averages is 1000 and for (b), the number of averages is 100.

is more reliable than the one achieved by the E5052B measurement bench. Moreover, the performances of the reference OCXOs used in the home-made dual-channel bench are close to the phase noise level of the device under test (DUT). As a consequence, no roll-off and bumps are observed on the measurement. The discrepancy level between the two measurements is about 10 dB in the worst case. This highlights the difficulty and precautions to take in order to measure such high-spectral purity signals. Measurements presented in the following were obtained with the best XM16-265 module.

Figure 7 plots absolute phase noise performances of key signals of the synthesis chain at 100 and 4596 MHz. In addition, it shows the absolute phase noise of the 9.192 GHz signal measured in Ref. 20, reported at 4.596 GHz ( $-6$  dB) for comparison. The absolute phase noise of the 100 MHz OCXO ideally multiplied to 4.596 GHz is also plotted to highlight limitations of the synthesis chain. The phase noise spectrum of the free-running 100 MHz Pascall OCXO has been measured at the level of  $-143$ ,  $-167$ , and  $-175$  dB rad<sup>2</sup>/Hz at 100 Hz, 1 kHz, and 50 kHz offset frequencies, respectively.

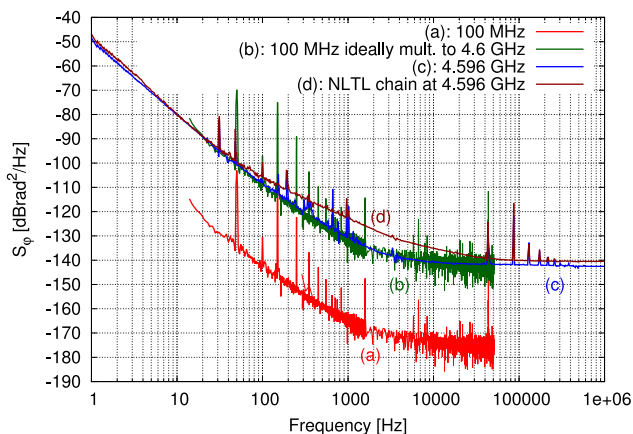


FIG. 7. Absolute phase noise performances of key signals of the Cs clock synthesis chain. (a) 100 MHz OCXO, (b) 100 MHz OCXO ideally multiplied to 4.6 GHz, (c) 4.596 GHz, and (d) 4.596 GHz signal extracted from the 9.192 GHz signal reported in Ref. 20.

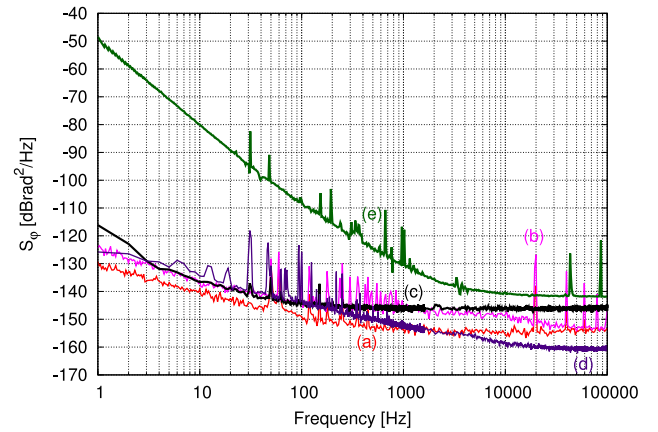


FIG. 8. Residual phase noise of key components of the Cs clock synthesis chain. The phase noise is given for the output frequency of each component. The absolute phase noise of the 4.596 GHz signal is also reported for reference. (a) Microwave mixer ZX05-14LH-S+ at 4.8 GHz, (b) frequency divider by 8 HMC363G8 (1.6 GHz-200 MHz), (c) frequency divider by 2 HMC361S8G (1.6 GHz-800 MHz), (d) residual noise of the frequency multiplication chain (1.6 GHz-4.8 GHz), and (e) absolute phase noise of the 4.596 GHz output signal.

The 4.596 GHz signal phase noise is measured to be  $-109$ ,  $-131$ ,  $-141$ , and  $-142$  dB rad<sup>2</sup>/Hz at 100 Hz, 1 kHz, 10 kHz, and 100 kHz, respectively. These results are in good agreement with perfect frequency multiplication of the initial OCXO 100 MHz signal.

The phase noise of the 4.8 GHz signal is measured to be identical to the 4.596 GHz but is not reported here for clarity of the figure. For offset frequencies from 100 Hz to 100 kHz, a critical region to be optimized in order to reduce the Dick effect contribution in vapor-cell atomic clocks, phase noise performances of the 4.596 GHz output signal are 2–8 dB better than performances measured in Ref. 20 reported at the same carrier frequency. Additionally, the white noise floor is also improved by about 2 dB.

For additional information, Fig. 8 reports residual phase noise performances of key components of the synthesis chain. The residual phase noise of the 1.6-4.8 GHz chain (Fig. 8, curve (d)) is shown to be clearly lower than the absolute phase noise of the output 4.596 GHz (Fig. 8, curve (e)). This confirms that the frequency multiplication chain allows to transfer the spectral purity of the 100 MHz OCXO without degradation.

### C. Residual frequency stability

The experimental setup shown in Fig. 9(a) was implemented to measure the residual frequency stability of 1.6-4.596 GHz frequency multiplication chains. A common 1.6 GHz signal from the XM16-265 module is split into two arms and sent in two identical 1.6-4.596 GHz chains. Output signal frequencies at 4.5959 and 4.5975 GHz are mixed to generate a beatnote at 1.6 MHz that is low-pass filtered and counted with a Symmetricom 5125A phase meter. The latter is driven by the 100 MHz signal of the XM16-265 module.

Figure 9(b) reports the measured relative frequency stability of the beatnote and the expected computed residual frequency stability of a single synthesis chain using a formula

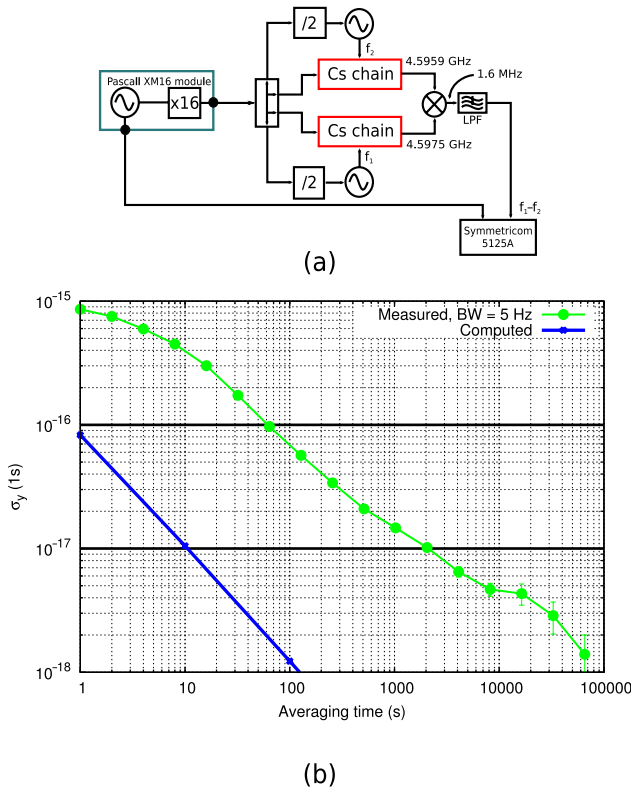


FIG. 9. (a) Experimental setup used for measurement of the Cs clock synthesis chains residual frequency stability and (b) relative frequency stability of the 1.6 MHz beatnote between two 1.6-4.8 GHz synthesis chains. The measurement bandwidth is 5 Hz. The phase noise of a single synthesis chain has been taken into account for the computed relative frequency stability.

converting flicker phase noise into Allan deviation.<sup>30</sup> The residual frequency stability is measured to be  $8 \times 10^{-16}$  and  $4.5 \times 10^{-18}$  at 1 s and 10 000 s averaging time, respectively, with a measurement bandwidth of 5 Hz.

As shown in Ref. 31, the power spectral density (PSD) of phase fluctuations of a signal can be expressed by the power law model  $S_\phi(f) = \sum_{i=0}^{-4} b_i f^i$  and then, according to Fig. 8, the residual flicker noise is at the level of  $b_{-1} = -123$  dB rad<sup>2</sup>/Hz, yielding a computed stability of  $8 \times 10^{-17} \times \tau^{-1}$  at 1 s with

a measurement bandwidth of 5 Hz. These performances can be considered as the ultimate performances achievable by the synthesis chain.

The differences we observe between this value and the measured residual frequency stability are related to environmental parameters (mainly temperature and humidity) that degrade the performances. In our application, the control of these parameters is not required since the measured performances are one order of magnitude below the Dick effect contribution.

### III. SYNTHESIS CHAIN FOR THE POP RB CELL CLOCK

#### A. Architecture of the synthesis chain

The architecture of the POP Rb cell clock synthesis chain is based on the same principle and shown in Fig. 10. The key driver is the low noise 100 MHz-1.6 GHz XM16 Pascall module. The 1.6 GHz signal is power-split into four arms. In the first arm, the 1.6 GHz signal is frequency-multiplied by 4 with a low-noise frequency multiplier (HMC917LP3E). The 6.4 GHz signal is band-pass filtered, isolated, and amplified with a microwave amplifier (Hittite HMC606) and sent to the LO port of a microwave mixer. In the second arm, the 1.6 GHz signal is frequency-divided to 400 MHz with a frequency divider (Hittite HMC365) and bandpass-filtered. In the third arm, the 1.6 GHz signal is frequency-divided by two (Hittite HMC361) and, then, bandpass filtered. The 800 MHz signal is used to drive a DDS (AD9910) with a power of 3 dBm. The DDS synthesizes 34.7 MHz at 0 dBm that is mixed with the 400 MHz signal by a double-balanced mixer to generate a 434.7 MHz signal. The latter signal is bandpass-filtered with a 10 MHz-bandwidth surface acoustic wave (SAW) filter (Golledge MA09629). In a last step, both 6.4 GHz and 434.7 MHz signals are mixed (Minicircuits ZX05-14LH-S+) to generate a 6.834 MHz signal. The latter is bandpass filtered, isolated, amplified to a power of about 0 dBm with a microwave amplifier (Hittite HMC606) and isolated. This output signal is used to interrogate the atomic resonance in the POP Rb clock experiment.

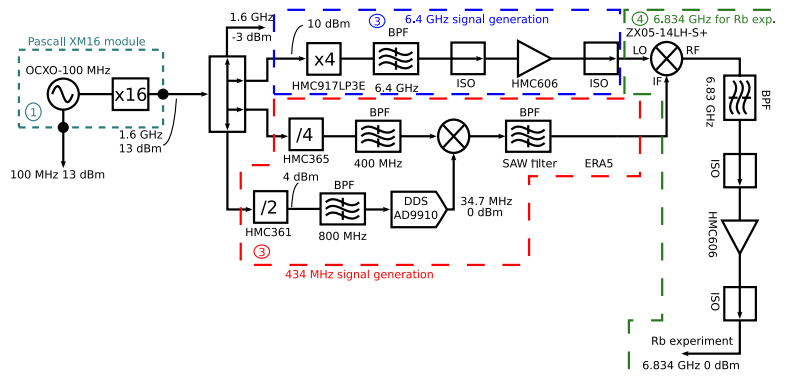


FIG. 10. Architecture of the frequency synthesis chain for the Rb cell clock. 4 main blocks are indicated on the diagram for better understanding. 1: The XM16 Pascall module that integrates a high-performance OCO and a 100 MHz-1.6 GHz frequency multiplication stage, 2: generation of a 6.4 GHz signal through frequency multiplication by 4 of the 1.6 GHz signal, 3: generation of a 434 MHz signal, 4: generation of a 6.834 GHz signal reference, filtering, and amplification. BPF: bandpass filter. ISO: isolator.

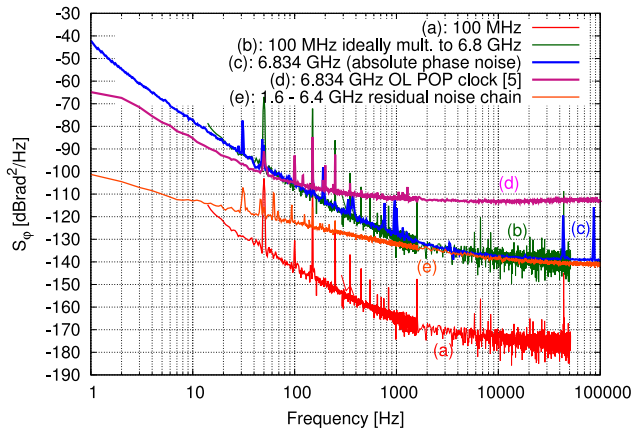


FIG. 11. Absolute phase noise performances of 100 MHz (a) and 6.834 GHz (c) signals of the Rb synthesis chain. The absolute phase noise of the ideally multiplied 100 MHz OCXO at 6.834 GHz is reported (b). Results at 6.834 GHz are compared with those reported in Ref. 5 (d). The residual phase noise of the 1.6-6.4 GHz frequency synthesis chain is given for information (e).

## B. Phase noise performances

Figure 11 plots absolute phase noise performances of the 100 MHz, 6.834 GHz signals of the Rb synthesis chain. These results are compared with those previously obtained in Ref. 5 and reported at the same carrier frequency. The absolute phase noise of the 100 MHz OCXO referred to a carrier of 6.8 GHz is shown for comparison. Additionally, the residual phase noise of the 1.6-6.4 GHz chain is given. The absolute phase noise at 6.834 GHz is  $-105$  dB  $\text{rad}^2/\text{Hz}$  and  $-138$  dB  $\text{rad}^2/\text{Hz}$  at 100 Hz and 10 kHz offset frequencies, respectively. Figure 11 demonstrates that the spectral purity of the 100 MHz OCXO is reported to 6.834 GHz without excess noise from the synthesis chain, except for a minor degradation on the white noise floor. Compared to the previous synthesis used in INRIM,<sup>5</sup> the phase noise floor is reduced by 28 dB while the phase noise is improved by about 5 dB at  $f = 230$  Hz, corresponding to the cycle frequency of the POP clock. In the synthesis developed in Ref. 5, the pilot source was a 10 MHz quartz oscillator. For this reason, phase noise performances reported in Ref. 5 are better for  $f < 100$  Hz and worse for  $f > 100$  Hz. Figure 12 shows the phase noise of signals at 400 and 800 MHz. The

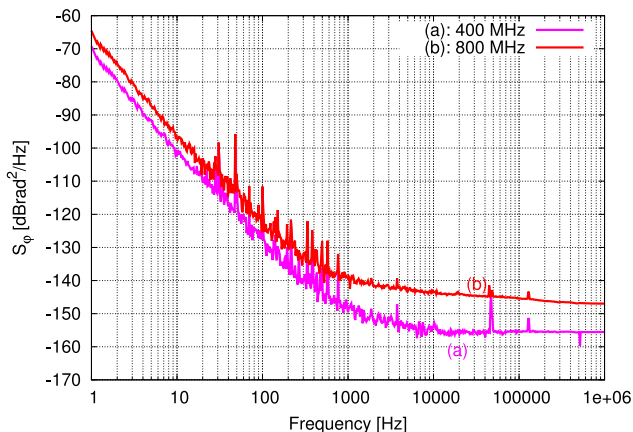


FIG. 12. Absolute phase noise of additional signals of the Rb synthesis chain. (a) 400 MHz. (b) 800 MHz.

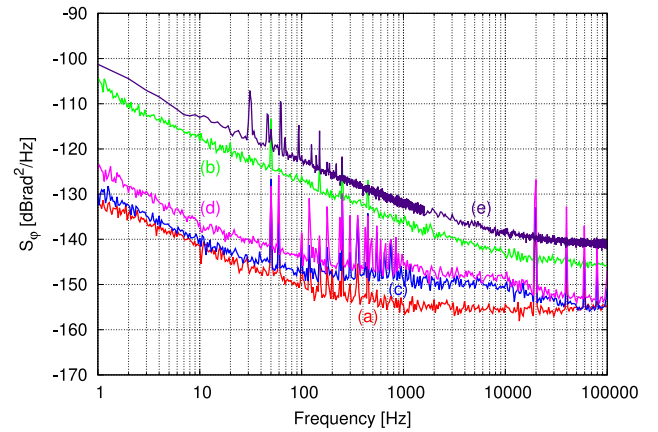


FIG. 13. Residual phase noise of key components of the Rb synthesis chain. (a) Microwave mixer, (b) 1.6-6.4 GHz frequency multiplier HMC917LP3E, (c) 1.6 GHz-400 MHz frequency divider HMC365G8, and (d) 1.6 GHz-800 MHz frequency divider HMC361S8G. The residual noise of the full 1.6-6.4 GHz synthesis chain is also reported (e).

difference between the phase noise level of the 400 MHz, 800 MHz, and 1.6 GHz confirms that the frequency division to sub-GHz frequencies is free from excess of noise for Fourier frequencies from 1 to 300 Hz. For higher offset frequencies, the residual noise of both dividers can limit the performances of the output signal. The white noise floor of both signals remains below the phase noise of the 6.8347 GHz signal.

Figure 13 reports the residual phase noise measurement of the Rb synthesis chain key components. The frequency multiplier HMC917LP3E—Fig. 13, curve (b) is identified to be the main phase noise contribution to the total residual noise of the synthesis chain (Fig. 13, curve (e)).

## C. Residual frequency stability

In Fig. 14, we report the measured and the computed residual relative frequency stabilities of the Rb clock synthesis chains. The residual frequency stability of the beatnote has been measured at the level of  $1.8 \times 10^{-15}$  at 1 s and  $1.8 \times 10^{-17}$  at 10 000 s.

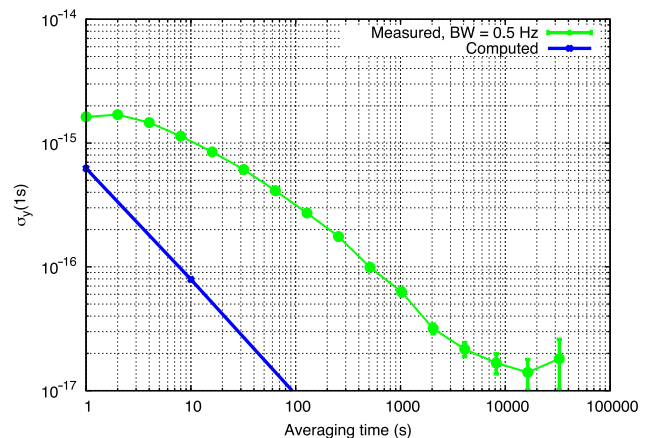


FIG. 14. Relative frequency stability of the 1.6 MHz beatnote between two 1.6-6.834 GHz synthesis chains. The measurement bandwidth is 0.5 Hz. In order to compute the relative frequency stability, a single synthesis chain has been considered.

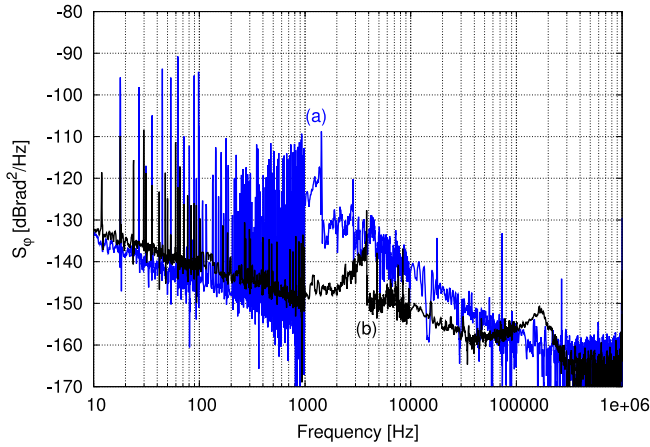


FIG. 15. Residual phase noise measurements of AD9914 (a) and AD9910 (b). For each DDS, the output and clock frequencies are 30 MHz and 800 MHz, respectively.

According to Fig. 13, the synthesis chain exhibits a flicker phase noise whose level is  $b_{-1} = -102$  dB rad<sup>2</sup>/Hz for  $f < 5$  kHz. This corresponds to a computed frequency stability for a single synthesis chain at the level of  $6 \times 10^{-16}$  at 1 s integration time with a  $\tau^{-1}$  slope.

#### IV. THE DIRECT DIGITAL SYNTHESIZER: REQUIREMENTS, CHOICE, AND PERFORMANCES

In synthesis chains, a DDS provides the fine tuning required to interrogate the clock transition. A drawback of this high-resolution is the generation of numerous frequency spurious related to the quantization noise.<sup>32</sup> The choice of this component is critical not to degrade the performances of the LO. In the new synthesis chain, the source pilot is a 100 MHz OCXO whereas it was a 10 MHz pilot in Ref. 5. Consequently, the white noise floor of the described synthesis chain is 20 dB lower than the one in Ref. 5. Additionally, the frequency generated by the DDS ( $\nu_{\text{DDS}}$ ) in the present Rb clock synthesis is 34 MHz, a factor 8 higher than in Ref. 5, leading to additional requirements of about 18 dB regarding to the white noise floor of the DDS. The phase noise scales proportionally to  $\nu_{\text{DDS}}^2$ . Thus, while the structure of the new synthesis is simpler, requirements in terms of phase noise for the DDS are more stringent by about 38 dB. We tested two DDSs for this work: AD9910 and AD9914. Figure 15 reports residual phase noise measurements of both DDSs for a clock frequency of 800 MHz and an output frequency of 30 MHz. The difference between both DDSs is related to their output digital-to-analog (DAC) converter: 12 bits for the AD9914 and 14 bits for the AD9910. Using the AD9910, the level of spurs is reduced by 10-12 dB. The spurs power is inversely proportional to the

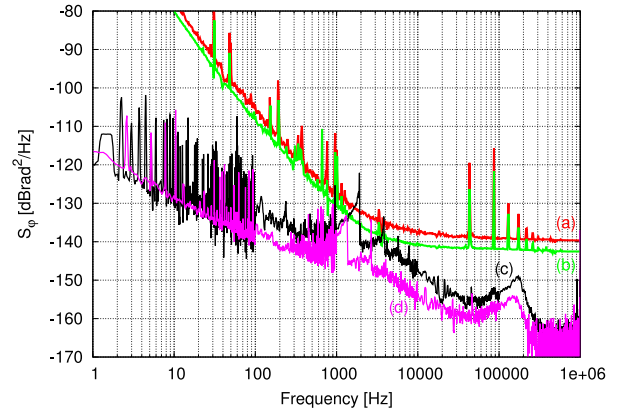


FIG. 16. Absolute phase noise of 6.834 GHz (a) and 4.596 GHz (b) signals. Comparison with the residual phase noise of the AD9910 with output frequency at 40 MHz (c) and 28 MHz (d).

clock frequency and is inversely proportional to the square of the resolution of the DAC. According to these results, the AD9910 is the best candidate for our application thanks to its high resolution and its high clock frequency (1 GHz maximum). Figure 16 reports on a same graph the residual phase noise of the AD9910 and absolute phase noise of both microwave signals. For  $1 \text{ kHz} < f < 10 \text{ kHz}$ , the effect of some spurs generated by the DDS is still visible. Nevertheless, the residual phase noise contribution of the DDS remains well below the absolute phase noise of output microwave signals. Spurs shown in the 1-10 kHz range can cause a slight degradation of the Dick effect contribution to the clock short term fractional frequency stability (about 25% at the maximum of the values reported in Table I).

#### V. DICK EFFECT CONTRIBUTION

In a pulsed atomic clock, the effect of the LO frequency noise can be characterized by the sensitivity function  $g(t)$ <sup>18</sup> which is the response of the atomic signal to a phase step of the interrogation oscillator at time  $t$ . The shape of  $g(t)$  depends on the atomic system and on the kind of interrogation used. The frequency stability limitation of an atomic clock due to the Dick effect is given by<sup>18</sup>

$$\sigma_{yLO}^2(\tau) = \frac{1}{\tau} \sum_{i=1}^{\infty} \frac{g_i^2}{g_0^2} S_y(i/T_c) = \frac{1}{\tau} \sum_{i=1}^{\infty} \frac{g_i^2}{g_0^2} S_y(2if_m), \quad (1)$$

where  $S_y(f) = S_\varphi(f) \times \left(\frac{\nu_0}{f}\right)^2$  is the power spectral density (PSD) of fractional frequency fluctuations. The parameters  $g_i$  and  $g_0$  are defined from the sensitivity function  $g$ .<sup>18</sup>  $i/T_c$  are the harmonics of the interrogation frequency.

TABLE I. Dick effect contribution  $\sigma_{yLO}$  (1 s) of synthesis chains to the clock short-term frequency stability. Results vary slightly depending on the XM16 module used.

	Clock	XM16-264	XM16-265	XM16-266	Current POP LO	NLTL-based LO
Results for	Rb POP	$2.4 \times 10^{-14}$	$2.0 \times 10^{-14}$	$2.3 \times 10^{-14}$	$6.5 \times 10^{-14}$	...
fitted data	Cs CPT	$3.6 \times 10^{-14}$	$3.1 \times 10^{-14}$	$3.6 \times 10^{-14}$	...	$6.2 \times 10^{-14}$

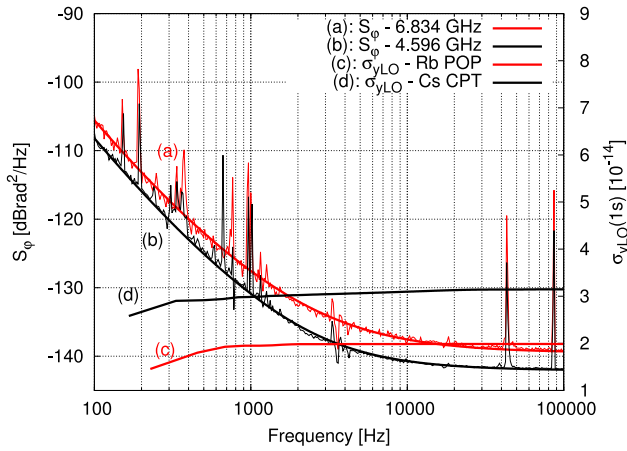


FIG. 17. Absolute phase noise at 6.834 GHz (a) and 4.596 GHz (b) [left axis] and expected Dick effect contribution [right axis] to the POP Rb (c) and CPT-based Cs (d) atomic clocks short term frequency stability.

Figure 17 summarizes the phase noise spectra of the 4.596 and 6.834 GHz frequency synthesizers, as well as the limits imposed by the Dick effect on the frequency stability of the corresponding atomic clocks. The use of the best module is considered (XM16-265). The Dick effect contribution is calculated using Eq. (1). For the Cs clock, operating parameters and conditions of the Ramsey pulsed sequence in the present study are a pumping time  $\tau_p$  of 2 ms and a free-evolution Ramsey time  $T$  of 4 ms, i.e., a clock cycle time  $T_c = \tau_p + T$  of 6 ms or clock cycle frequency  $f_c = 1/T_c = 166$  Hz. For the Rb POP clock, the Ramsey sequence uses an interaction time  $\tau_i = 0.4$  ms, a free-evolution time  $T = 3$  ms, a pumping time  $\tau_p = 0.4$  ms and a detection time  $\tau_d$  of 0.15 ms, inducing a cycle time  $T_c = 2\tau_i + T + \tau_p + \tau_d = 4.35$  ms,<sup>5</sup> i.e., a clock cycle frequency of 230 Hz. The Dick effect contribution is plotted as a function of the noise integration bandwidth, starting at the offset frequency  $f = f_c$ . Once this integrated noise stops to contribute to the Dick effect,  $\sigma_y$  reaches a floor that is the total Dick effect contribution. For the Cs cell clock, the Dick effect contribution is reported at the level of  $3.1 \times 10^{-14}$  at 1 s, while this limitation was estimated at  $6.2 \times 10^{-14}$  for the synthesis architecture reported in Ref. 20 and  $2.7 \times 10^{-13}$  in Ref. 7. For the Rb POP clock, the Dick effect contribution is reported at the level of  $2 \times 10^{-14}$  at 1 s, a value close to the atomic clock shot noise limit.<sup>5</sup>

The Dick effect contribution has been estimated for synthesis chains using each XM16 module. Table I summarizes expected performances for each configuration. The computation has been performed by fitting each phase noise spectrum data set by the power-law function such as  $S_\varphi(f) = \sum_{i=0}^4 b_i f^i$ . All configurations are compatible with the development of a high-performance vapor cell atomic clock.

## VI. CONCLUSIONS

We reported the development and phase noise characterization of 4.596 GHz and 6.834 GHz microwave frequency synthesizers devoted to be used as local oscillators in compact Cs and Rb vapor-cell atomic clocks. These synthesizers are

based on frequency multiplication of a high spectral purity 100 MHz OCXO with a key step at 1.6 GHz using a custom-designed low-noise frequency-multiplication module. Absolute phase noise performances of the 4.596 GHz signal are  $-131$  dB rad<sup>2</sup>/Hz and  $-141$  dB rad<sup>2</sup>/Hz at 1 kHz and 10 kHz offset frequencies, respectively. For the 6.834 GHz signal, they are  $-128$  dB rad<sup>2</sup>/Hz and  $-138$  dB rad<sup>2</sup>/Hz at 1 kHz and 10 kHz offset frequencies, respectively. These performances allow to reject the Dick effect contribution to the short-term frequency stability of CPT Cs and Rb POP vapor-cell atomic clocks at the level of  $3.1 \times 10^{-14}$  and  $2 \times 10^{-14}$ , respectively. These values are close to the atomic clock shot noise limit. Residual phase noise performances of main components of the synthesizers were measured and reported to evaluate main limitations. The residual frequency stability of the synthesis chains were measured to be at the  $10^{-15}$  level for 1 s integration time. The characterization of two different DDSs and their impact on the synthesis phase noise performances was reported.

## ACKNOWLEDGMENTS

This work has been funded by the EMRP program (IND55 Mclocks). The EMRP is jointly funded by the EMRP participating countries within EURAMET and the European Union. This study was partly supported by LNE and LabeX FIRST-TF. The authors thank J. M. Danet (Syrlinks) and S. Guérandel (LNE-SYRTE) for simulations of the Dick effect contribution to the atomic clock frequency stability. The authors acknowledge G. Thorp (Pascall Electronics) and E. Rubiola (FEMTO-ST) for stimulating discussions.

<sup>1</sup>See <http://www.spectratime.com/products> for information on performances of Rb Clocks (Spectratime).

<sup>2</sup>See <http://www.microsemi.com/> for information on performances of Rb Clocks (Microsemi).

<sup>3</sup>T. Bandi, C. Affolderbach, C. Stefanucci, F. Merli, A. K. Skrivervik, and G. Milet, *IEEE Trans. Ultrason., Ferroelectr., Freq. Control* **61**(11), 1769 (2014).

<sup>4</sup>S. Kang, M. Gharavipour, C. Affolderbach, F. Gruet, and G. Milet, *J. Appl. Phys.* **117**, 104510 (2015).

<sup>5</sup>S. Micalizio, C. E. Calosso, A. Godone, and F. Levi, *Metrologia* **49**, 425 (2012).

<sup>6</sup>J. Vanier, *Appl. Phys. B* **81**, 421 (2005).

<sup>7</sup>J. M. Danet, M. Lours, S. Guérandel, and E. De Clercq, *IEEE Trans. Ultrason., Ferroelectr., Freq. Control* **61**(4), 567 (2014).

<sup>8</sup>Y. Y. Jau, E. Miron, A. B. Post, N. N. Kuzma, and W. Happer, *Phys. Rev. Lett.* **93**(16), 160802 (2004).

<sup>9</sup>X. Liu, J. M. Mérolla, S. Guérandel, C. Gorecki, E. De Clercq, and R. Boudot, *Phys. Rev. A* **87**, 013416 (2013).

<sup>10</sup>X. Liu, J. M. Mérolla, S. Guérandel, E. De Clercq, and R. Boudot, *Opt. Express* **21**(10), 12451-12459 (2013).

<sup>11</sup>M. Abdel Hafiz and R. Boudot, "Preliminary results of a Cs vapor-cell CPT clock using push-pull optical pumping," in *Proceedings of the IEEE EFTF-IFCS Conference Joint Meeting, 13-17 April 2015, Denver, Colorado* (IEEE, 2015), pp. 71-73.

<sup>12</sup>F. X. Esnault, D. Holleville, N. Rossetto, S. Guérandel, and N. Dimarcq, *Phys. Rev. A* **82**, 033436 (2010).

<sup>13</sup>F. X. Esnault, E. Blanshan, E. N. Ivanov, R. E. Scholten, J. Kitching, and E. Donley, *Phys. Rev. A* **88**, 042120 (2013).

<sup>14</sup>See <http://www.t4science.com/products/> for information on performances of passive hydrogen masers (T4Science).

<sup>15</sup>G. Kramer, in *Digest of the Conference on Precision Electromagnetic Measurements (CPEM), London, UK* (IEEE, 1974), pp. 157-158.

<sup>16</sup>C. Audoin, V. Candelier, and N. Dimarcq, *IEEE Trans. Instrum. Meas.* **40**(2), 121 (1991).

- <sup>17</sup>G. J. Dick, in *Proceedings of Precise Time and Time Interval, Redondo Beach, CA* (US Naval Observatory, 1987), pp. 133–147.
- <sup>18</sup>C. Audoin, G. Santarelli, A. Makdissi, and A. Clairon, *IEEE Trans. Ultrason., Ferroelectr., Freq. Control* **45**, 887 (1998).
- <sup>19</sup>See <http://www.inrim.it/Mclocks/> for information on the MClocks project.
- <sup>20</sup>B. François, C. E. Calosso, J. M. Danet, and R. Boudot, *Rev. Sci. Instrum.* **85**, 094709 (2014).
- <sup>21</sup>R. Boudot, S. Guérandel, and E. de Clercq, *IEEE Trans. Instrum. Meas.* **58**(10), 3659 (2009).
- <sup>22</sup>See <http://www.pascall.co.uk/> for information on performances of quartz crystal oscillators and multiplication chains developed by Pascall electronics.
- <sup>23</sup>E. Rubiola and V. Giordano, *IEEE Trans. Ultrason., Ferroelectr., Freq. Control* **51**, 15 (2007).
- <sup>24</sup>R. L. Filler and J. R. Vig, in *IEEE 34th Annual Symposium on Frequency Control* (IEEE, 1980), p. 187.
- <sup>25</sup>P. Yun, J. M. Danet, D. Holleville, E. De Clercq, and S. Guérandel, *Appl. Phys. Lett.* **105**, 231106 (2014).
- <sup>26</sup>E. Rubiola and V. Giordano, *Rev. Sci. Instrum.* **71**(8), 3085 (2000).
- <sup>27</sup>E. Rubiola and R. Boudot, *IEEE Trans. Ultrason., Ferroelectr., Freq. Control* **54**(5), 926-937 (2007).
- <sup>28</sup>C. W. Nelson, A. Hati, and D. Howe, *Rev. Sci. Instrum.* **85**, 024705 (2014).
- <sup>29</sup>F. Walls, in *IEEE 46th Annual Symposium on Frequency Control* (IEEE, 1992), pp. 257-261.
- <sup>30</sup>E. Rubiola, *Phase Noise and Frequency Stability in Oscillators* (Cambridge University Press, 2008).
- <sup>31</sup>E. Parker, in *IEEE 41st Annual Symposium on Frequency Control* (IEEE, 1987), pp. 99-110.
- <sup>32</sup>C. E. Calosso, Y. Gruson, and E. Rubiola, “Phase noise and amplitude noise in DDS,” in *Frequency Control Symposium (IEEE FCS)* (IEEE, 2012), pp. 1-6.